

A Kinetic Investigation of Triacetin Methanolysis and Assessment of the Stability of a Sulfated Zirconium Oxide Catalyst

Rafael L. Temóteo¹ · Marcio J. da Silva¹ · Fabio de Ávila Rodrigues¹ · Wagner F. da Silva¹ · Deusanilde de Jesus Silva¹ · Cesar M. Oliveira¹

Received: 18 February 2018 / Revised: 3 May 2018 / Accepted: 4 May 2018
© 2018 AOCS

Abstract In this work, the activity and stability of a sulfated zirconium catalyst in transesterification reactions of triacetin, a model molecule, were investigated. This catalyst has Lewis and Brønsted acid sites and has shown to be highly active in reactions converting triacetin into methyl esters. This catalyst was synthesized using the impregnation method, and systematically characterized using the techniques of x-rays diffraction (XRD), scanning electron microscopy, Fourier transform-infrared spectroscopy (FT-IR), Brunauer, Emmett, and Teller, and thermal gravimetry analysis (TGA). Kinetic studies were carried out to determine the activation energy as well as the reaction order. The effects of the main reaction parameters, such as temperature, the molar ratio, and the catalyst content, were evaluated. The reuse and possible leaching of the catalyst were also investigated. The highest efficiency (ca. 99% of methyl esters) was achieved in the sulfated zirconium oxide-catalyzed transesterification reaction.

Keywords Sulfated zirconium oxide · Lewis and Brønsted acid sites · Triacetin · Transesterification

J Am Oil Chem Soc (2018).

Supporting information Additional supporting information may be found online in the Supporting Information section at the end of the article.

✉ Marcio J. da Silva
silvamj2003@ufv.br

¹ Chemistry Department, Federal University of Viçosa, University Campus, P.H. Rolfs Avenue, Viçosa, Minas Gerais 36570-000, Brazil

Introduction

The depletion of fossil fuels has motivated the search for alternative energy sources. Biodiesel obtained from renewable raw materials reduces the emission of greenhouse gases, and is environmentally friendly. Nonetheless, the traditional processes of biodiesel production are carried out under homogeneous alkaline catalysis conditions, which generate large amounts of effluents and neutralization residues (Ilmi, Hommes, Winkelman, Hidayat, & Heeres, 2016). Conventional alkaline processes require the control of the amount of free fatty acids (FFA) to avoid the undesirable saponification reactions (Nakatake, Yazaki, Matsushima, & Ohshima, 2016). Therefore, only raw materials with low content of fatty acids can be used in the alkaline processes

To solve these problems, an attractive alternative is to replace the homogeneous catalysts with solid acid catalysts, which are compatible with lipidic raw materials and are recyclable catalysts (Grossi, Jardim, de Araújo, Lago, & da Silva, 2010; Silva, Laier, & da Silva, 2010). These solid catalysts simplify the process because they make the separation steps of alkyl esters easier and avoid the need for neutralization steps (Grossi et al., 2010; Zabeti, Daud, & Aroua, 2009). A variety of solid acids have already been tested for the synthesis of methyl esters through esterification reactions of FFA and transesterification of triglycerides (Zabeti et al., 2009; Zieba, Drelinkiewicz, Chmielarz, Matachowski, & Stejskal, 2010). Amberlyst-15 resins (Pradhan, Chakraborty, & Chakraborty, 2016), zeolites (Wang & Chen, 2016), carbon-based biomass (Mardhiah, Ong, Masjuki, Lim, & Pang, 2017), and polyaniline sulfate (Intarapong, Luengnaruemitchai, & Jai-In, 2012) are some examples.

In this sense, despite low acidity and small porosity and surface area, zirconium oxide has received a lot of attention

due to its high thermal and chemical stability (Lughi & Sergo, 2010; Miao et al., 2017; Ranjbar, Yousefi, Lahooti, & Malekzadeh, 2012; Sigwadi, Mavundla, Moloto, & Mokrani, 2016). The low acidity and surface area can be improved by different strategies. The treatment of ZrO_2 with sulfuric acid allows an increase in catalytic activity of this material, making it a superacid material (Silva, Moura, Silva, Pallone, & Costa, 2017).

The superacidity of ZrO_2 is attributed to the formation of several Brønsted and Lewis acid sites on its surface. Meanwhile, the Lewis acid sites appear due to the electron withdrawing effect of the sulfate anions on the zirconium cations, the Brønsted acid sites are formed by the presence of protons provided by the treatment with sulfuric acid (Silva et al., 2017). Conversely, the immobilization of ZrO_2 over solids with a high surface area makes them a highly active catalyst in several acid-catalyzed reactions (Bandyopadhyay, Tsunoji, & Sano, 2017; Delesma, Castillo, Sevilla-Camacho, Sebastian, & Muñiz, 2017). Starting from these two different approaches (i.e., sulfuric acid treatment or supporting on porous solids), some studies have demonstrated the efficiency of sulfated ZrO_2 as an efficient heterogeneous acid catalyst. Jitputti et al. (2006) investigated the transesterification of renewable feedstock such as palm kernel and crude coconut oils, and verified that high methyl ester yield (ca. 90% and 86%, respectively) was achieved with sulfated ZrO_2 . Although, when ZrO_2 was not sulfated, a strong decrease occurred in reaction yield (ca. 64% and 48% was obtained, respectively).

The combination of ZrO_2 with other metal oxides (i.e., WO_3 , Al_2O_3) was assessed by Jacobson, Gopinath, Meher, and Dalai (2008). No gains in terms of mechanical resistance were obtained, however, the catalytic activity was enhanced. Furuta, Matsushashi, and Arata (2006) investigated the combination of these three oxides (i.e., ZrO_2 , WO_3 , and Al_2O_3), as well as the effect of sulfuric acid treatment. These catalysts were used in transesterification reactions of soybean oil with methyl alcohol at temperatures ranging from 473 to 573 K. Tungsten-zirconium-alumina untreated oxide was found to have a higher activity in transesterification compared to the sulfated zirconium-alumina oxide catalyst. Park et al. also verified that the introduction of tungsten improved the stability of zirconium catalysts (Park, Chung, Eom, Lee, & Lee, 2010; Park, Dw, Kim, Lee, & Lee, 2008).

Model molecules such as triolein (Wang & Chen, 2016), triacetin (Park et al., 2010), and tricaprillin (Chantrasa, Phlernjai, & Goodwin, 2011) are useful to access the activity of solid acid catalysts. Unlike fatty materials, which contain glycerides with the carbon chains with different sizes, these materials present chemical and structural simplicity, facilitating the identification and quantification of reaction products.

In this work, we have assessed the catalytic activity of sulfated zirconium oxide in transesterification reactions of

triacetin with methyl alcohol. We paid special attention to the main reaction parameters such as temperature, reactant stoichiometry, and catalyst concentration. A kinetic study provided the activation energy and the reaction order. The stability of the catalyst was evaluated as well as its ability to be recycled.

Materials and Methods

Chemicals

All chemicals and solvents were used as received. Zirconium hydroxide was purchased from Sigma–Aldrich (St. Louis, Missouri, EUA) (97 wt%). Triacetin (98 wt%) was provided by Buschle and Lepper S.A. (Joinville, Brazil), ammonium sulfate (99 wt%) was bought from Synth S.A. (Sao Paulo, Brazil), methyl alcohol (99.8 wt%) was from Vetec (Sao Paulo, Brazil). Acetone (99.8 wt%) was purchased from Alphatec (Sao Paulo, Brazil).

Synthesis of the Catalyst

The catalyst was synthesized using the impregnation method. Zirconium hydroxide (ca. 10 g, 31 mmol) was impregnated with 0.5 M ammonium sulfate solution and incubated for 18 hours. It was then oven dried for 12 hours and then calcined at 873 K for 4 hours according to Sun et al. (2005).

Characterization of Catalysts

Crystalline states of the zirconium catalyst were determined using a diffractometer model D8-Discover (Billerica, MA, US) using $\text{Cu-K}\alpha$ ($\lambda = 15,405 \text{ \AA}$) operating at 40 kV and mA. The patterns were recorded from 5° to 50° at a scanning rate of 4° min^{-1} . FT-IR spectra were recorded on a Varian 660 FT-IR spectrophotometer (P.A. California, US) in the wavenumber range $4000\text{--}400 \text{ cm}^{-1}$.

Nitrogen adsorption–desorption isotherms were measured at 77 K using a Micromeritics 2010 instrument (Norcross, G.A., US). The pore-size distribution was calculated from the desorption isotherm obtained using the Barrett, Joyner, and Halenda method. Surface area was determined using desorption–adsorption isotherms of nitrogen (Brunauer, Emmett, and Teller [BET]) in an ASAP 2010 Micromeritics instrument (Norcross, Georgia, USA).

The thermal decomposition temperatures and weight loss were measured in a Differential Thermal Gravimetry (DTG)-60H Perkin Elmer Thermal Gravimetry Analysis (TGA)/Differential Scanning Calorimetry (DSC) analyzer (Waltham, Massachusetts, EUA) at a heating rate of 20 K min^{-1} under

a nitrogen atmosphere from room temperature till 1273 K. The samples were scanned from room temperature to 873 K at a heating rate of 10 K min⁻¹ under a nitrogen atmosphere. The catalyst morphology was characterized using scanning electron microscopy (SEM) equipped with an energy-dispersive X-ray spectroscopy (EDS) unit (JEOL [Akishima, Tóquio, Japão], JSM-6010A).

Catalyst acidity was measured by potentiometric titration, in agreement with the procedure reported by Pizzio, Vásquez, Cáceres, and Blanco (2003). The electrode potential variation was measured with a potentiometer (i.e., Bel, model W3B [Sao Paulo, Brazil]). Typically, a solution containing an adequate amount of heteropolyacid (HPA) dissolved in CH₃CN was titrated with *n*-butylamine solution in toluene (ca. 0.025 mol L⁻¹).

Catalytic Tests

The sulfated zirconia catalyst, (SZr), was evaluated in transesterification reactions of triacetin with methyl alcohol. The experiments were carried out in a 300 mL Parr reactor (model 4848, Parr Instrument Company, Moline, IL, US) equipped with a mechanical stirrer and heated to 393 K over 1 hour under autogenic pressure.

The effects of the main reaction parameters were evaluated as follows. To assess how the proportion of reactants affects the reaction, we have performed runs with five different stoichiometries of methyl alcohol to triacetin (ca. 3:1, 6:1, 9:1, 12:1, and 20:1). In these tests, the temperature was kept constant (ca. 393 K) and the catalyst load was ca. 5 wt%. The temperature effects were assessed performing reactions at five levels (ca. 343, 363, 383, 393, and 403 K). On these runs, the molar proportion between methyl alcohol and triacetin was 20:1 and the catalyst load was ca. 5 wt%. Finally, the effect of the catalyst concentration was studied in the load range of 1–5 wt%; these reactions were carried out at 1:20 proportion of triacetin to methyl alcohol and at 393 K.

Reaction Monitoring and Product Identification

The reaction progress was followed by gas chromatography analyses using a Shimadzu gas chromatograph equipped with a flame-ionization detector and a capillary column (Restek [Bellefonte, PA, US], 30 m × 0.25 mm × 0.25 μm). The carrier gas was H₂ with a flow of 2.0 mL min⁻¹. The temperature profile was as follows: an initial temperature of 333 K, a heating rate of 5 K min⁻¹ until 373 K; 10 K min⁻¹ to 443 K; 5 K min⁻¹ until 483 K, kept constant for 2 min. The injector and detector temperatures were 333 and 483 K, respectively. To calculate the reaction yields, Eq. 1 was used.

$$\text{Conversion}(\%) = \frac{A_0 - A}{A_0} \times 100\% \quad (1)$$

Herein, “A₀” is the initial area of the triacetin GC peak, obtained from the calibration curve; “A” is the area of the triacetin GC peak present in the chromatogram. The reaction products were identified with coinjection of pure samples and gas chromatography-mass spectrometry (GC-MS) analysis (Shimadzu 2010, 70 eV).

Reuse and Recycling of Catalysts; Leaching Tests

To evaluate the reuse and the leaching of the SZr catalyst, the following procedure was used; after the end of the reaction, the solid catalyst was filtered, washed with acetone, and dried in an oven at 383 K for 5 hours. Afterward, it was weighed and reused in another catalytic run. The FT-IR spectra, the diffractograms, and the micrographs of the washed samples were recorded prior to the sulfate leaching test and the elemental analysis.

Results and Discussion

Catalyst Characterization

X-Ray Diffraction

Fig. 1 presents the diffractograms of the starting sample (i.e., Zr(OH)₄ (a) and ZrS catalyst (b)).

The literature describes that the main diffraction lines of pure ZrO₂ rise at 2θ values matching the Joint Committee on Powder Diffraction Standards data mixed of monoclinic and tetragonal structures. They are present at 2θ = (28.2°, 31.4°, and 34.0°) and 2θ = (30.2°, 35.2°, 50.6°, and 60.2°), respectively (Basahel, Ali, Mokhtar, & Narasimharao, 2010).

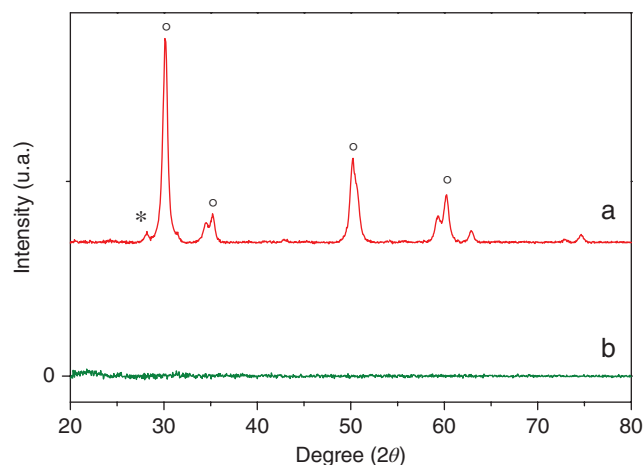


Fig. 1 Powder X-ray diffraction patterns of samples sulfated zirconium oxide (a) and zirconium hydroxide (b); the tetragonal phase (°) and the monoclinic phase (*)

As shown in Fig. 1, all these characteristic peaks of the tetragonal ($^{\circ}$) and monoclinic phases (*) are present in the diffractogram of the SZr catalyst (Fig. 1). Such peaks are in accordance with the synthesis and characterization of SZr previously described (Basahel et al., 2010; Dosuna-Rodríguez, Adriany, & Gaigneaux, 2011; Son, Gwon, & Kim, 2001). According to Brum, Santos, Destro, and Guerreiro (2011), the tetragonal phase is very desirable in SZr, because it has high acid strength and, consequently, may result in great catalytic activity.

SEM Images

Fig. 2 shows the SEM images of commercial zirconium hydroxide and sulfated zirconium samples. It is possible to observe that the sample of $Zr(OH)_4$ has low conduction of

electrons (Fig. 2a,b), inducing a charge accumulation, not showing roughness or porosity on its surface. Conversely, the samples of the SZ catalyst (Fig. 2c,d) show a morphology formed by larger-sized particles and pores on their surface. Structures like these are found in the literature (Pereira, Júnior, Carvalho, & Silva, 2015; Shi et al., 2016).

FT-IR Analysis

The FT-IR spectrum of SZ (Fig. SP1) shows an absorption band of low intensity in the region of $3600\text{--}3000\text{ cm}^{-1}$; this band is assigned to the deformation (δ HOH) of water molecules associated with the sulfate group (Ivanova, Harizanova, Koutzarova, & Vertruyen, 2010). In addition, we can see that the sulfated ZrO_2 showed bands at 1620 and 3400 cm^{-1} wavenumbers; the first one is attributed to the

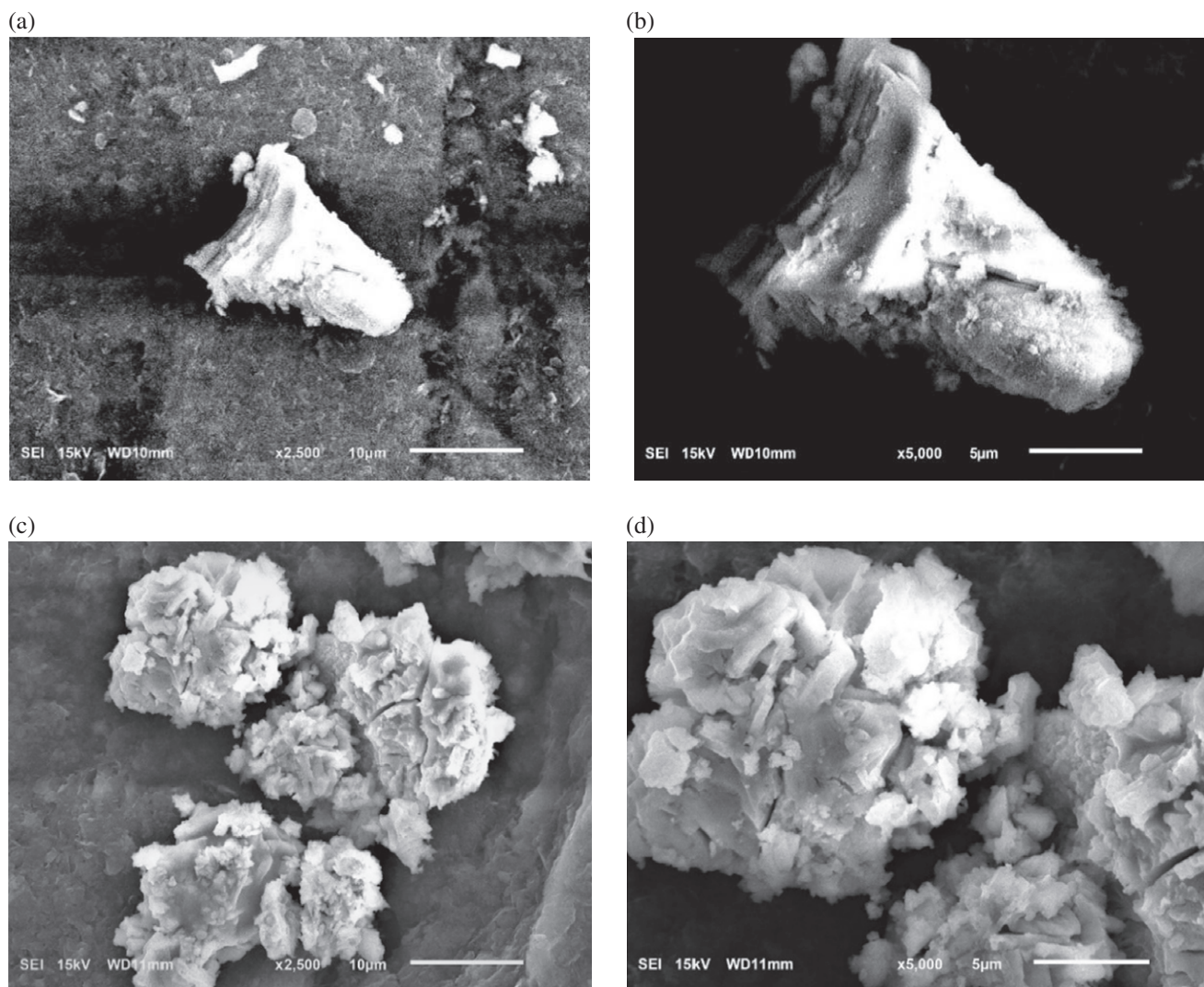


Fig. 2 SEM images of $Zr(OH)_4$ samples, 2500 times magnified (a), 5000 times magnified (b), and sulfated zirconium, 2500 times magnified (c), 5000 times magnified (d)

scissor bending mode of water molecules coordinated to the Zr^{4+} cations. The second band was assigned to the vibrations of physically adsorbed hydroxyl groups to the Zr^{4+} cations (Heshmatpour & Aghakhanpour, 2011; Jayakumar et al., 2011).

A higher intensity for this same absorption band can be verified in the zirconia hydroxide spectrum (Fig. SP1). According to Yu et al. (2012), the absorption between 1000 and 1250 cm^{-1} wavenumbers is assigned to the vibrations of the S—O bonds of the sulfate groups bonded to the zirconium oxide surface (Fig. SP1). This band is absent in the starting material for this same region. The absorption bands located around $700\text{--}400\text{ cm}^{-1}$ correspond to the Zr—O—O—Zr bond deformation modes and Zr—O bond asymmetric stretching, which is very common in crystalline ZrO_2 (Hwang et al., 2003).

The absorption band at 1422 cm^{-1} wavenumber is referred to the absorption of nonbridging OH groups (Ibrahim, 2015). The stretching bands at 502 and 570 cm^{-1} are assigned to tetragonal and monoclinic structures of ZrO_2 , respectively (Rouquerol, Rouquerol, & Sing, 1999).

Surface Area and Porosity Properties

The pore-size distribution obtained from the desorption branch of the isotherms is shown in Fig. SP2. The specific surface area (S_{BET}), total volume, size, and distribution of pore diameter obtained from the N_2 adsorption–desorption isotherms were $36.3\text{ m}^2\text{ g}^{-1}$, $0.047\text{ cm}^3\text{ g}^{-1}$, and 18.46 \AA , respectively.

The isotherms of the sulfated zirconium oxide samples are stratifying as type II, which is a model of either a nonporous or a mixed pore system according to the International Union of Pure and Applied Chemistry (IUPAC) classification (Kamaruzaman & Chin, 2014).

Thermogravimetry Analyses

Fig. SP3 shows the TG curves of the SZr and $Zr(OH)_4$ samples. Both samples presented considerable losses of mass between 298 and 573 K, which were assigned to the dehydration and dehydroxylation processes (Saravanan, Tyagi, & Bajaj, 2014). However, between 873 and 1073 K, the SZr sample presented another significant loss of weight due to the decomposition of the sulfate groups (Garcia, Teixeira, Marciniuk, & Schuchardt, 2008). It is noteworthy that the mass loss suffered by the $Zr(OH)_4$ sample is higher than that observed on TG curve of the SZr, in the region of 298–573 K. This is evidence that $Zr(OH)_4$ contains more hydroxyl groups than the SZr sample. It was confirmed by the OH stretching band at wavelength 3100 cm^{-1} (Fig. SP3). All our results agree with the literature data (Garcia et al., 2008; Noda, Gonçalves, de Borba, & Silveira, 2007).

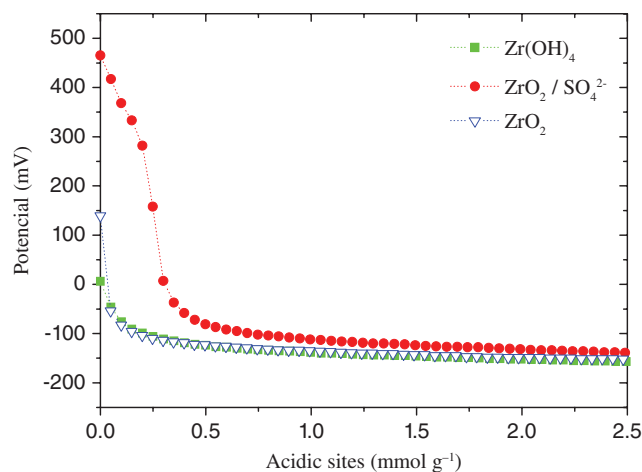


Fig. 3 Potentiometric titration with *n*-butylamine of the precursor and zirconium catalysts

To measure the acid strength of the zirconium catalysts, the samples were potentiometrically titrated with *n*-butylamine solution (Fig. 3). The initial electrode potential (E_i) allows classifying the acidity strength of acid sites as: $E_i > 100\text{ mV}$ (very strong sites), $0 < E_i < 100\text{ mV}$ (strong sites), $-100 < E_i < 0$ (weak sites), and $E_i < -100\text{ mV}$ (very weak sites) (Pizzio et al., 2003).

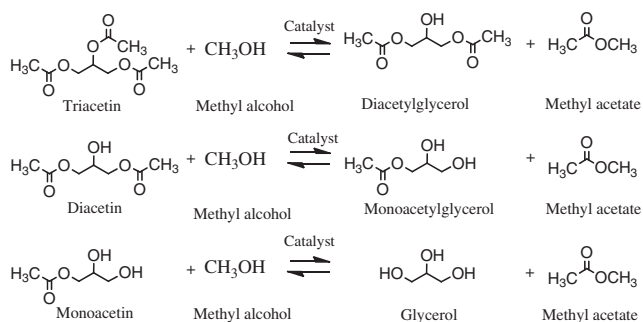
The potentiometric titration curves revealed that the treatment of the zirconium oxide catalysts with sulfuric acid was highly efficient. After the conversion of $Zr(OH)_4$ to ZrO_2 and their posterior treatment with sulfuric acid, the acid strength of the zirconium catalysts was notably increased. The initial electrode potential of 460 mV of the SZr samples indicates that these catalysts have very strong acid sites; conversely, their synthetic precursors have weak acid sites, as demonstrated by the initial electrode potential close to zero (Pizzio et al., 2003).

The Reactivity of Triglyceride and the Activity of the SZr Catalysts

Triacetin was used as a triglyceride model for the kinetic study of this reaction because it has the same chemical functionality as any triglyceride molecule, sharing the same reactivity principles. The transesterification of triacetin with methyl alcohol occurs in three sequential steps, as depicted in Scheme 1 (Muñiz, Castillo, Robles, & Sansores, 2016).

Due to the high steric hindrance, the acetyl group on the secondary carbon atom is more reactive than that on primary carbon atoms and consequently it was preferentially transesterified (Corma, 1997).

Initially, we have assessed the catalytic activity of zirconium oxide before and after the sulfuric acid treatment. The kinetic curves are displayed in Fig. SP4. These results



Scheme 1 Transesterification steps of triacetin with methyl alcohol

agree with the acidic properties of the catalysts; in Fig. 3, the zirconium oxide presented acidic sites weaker than sulfated zirconium oxide and in a lower amount.

Kinetic Studies

Effect of Temperature on SZr-Catalyzed Transesterification of Triacetin with Methyl Alcohol

To study the effect of the temperature on the reaction rate, we carried out catalytic runs at temperatures ranging from 343 to 423 K. Fig. 4a shows the kinetic curves obtained.

When carrying out catalytic runs at 343 K, no significant conversion was achieved, therefore, the curve was omitted in Fig. 4a. Although the reactions have displayed different initial rates, the runs performed at 403 and 423 K achieved almost a complete conversion after 1 hour of the reaction. These results are superior than those described by Bandyopadhyay et al. (2017), which studied the activity of ordered

Table 1 Rate constant and the correlation coefficient of curves of the $\ln(\text{instantaneous triacetin concentration})/(\text{initial triacetin concentration})$ as a function of reaction time

Temperature (K)	Rate constants (s^{-1})	R^2	$1/T$	$-\ln k$
343	0.003	0.98	2.915	-5.809
363	0.008	0.99	2.754	-4.828
383	0.0252	0.99	2.611	-3.681
403	0.0623	0.99	2.481	-2.776
423	0.1327	0.987	2.364	-2.019

mesoporous silicas (i.e., MCM-48, MCM-41, and SBA-15).

The profile of kinetic curves shows that an increasing of temperature resulted in a higher rate of reaction as well as a higher final conversion. These data provided the kinetic parameters to calculate the reaction order (see “Dependence of the Reaction Rate in Relation to the Triacetin Concentration”) and the activation energy (see “Effect of Catalyst Load on the SZr-Catalyzed Transesterification of Triacetin with Methyl Alcohol”).

Dependence of the Reaction Rate in Relation to the Triacetin Concentration

From the kinetic curves of Fig. 4a, it was possible to determine the specific reaction rate constants for each temperature. The dependence of the reaction rate on the concentration of triacetin was determined from plots of $\ln [A/A_0]$ as a function of the reaction time (Fig. 4b).

These experimental data were used to calculate the rate constant (k) using the first-order rate law. From the angular coefficients of the curves shown in Fig. 4b, the rate

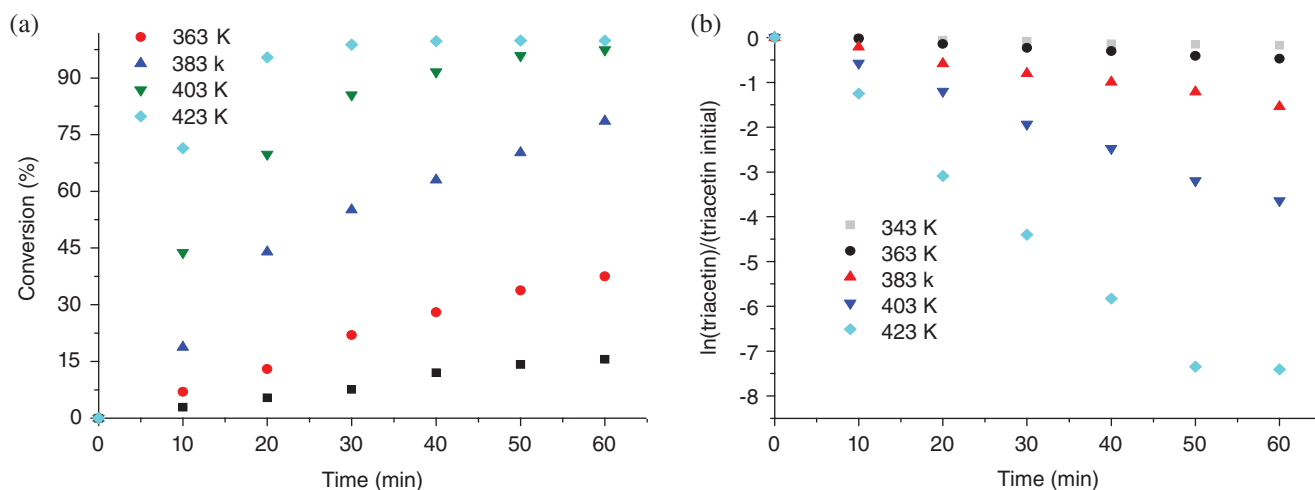


Fig. 4 Effect of temperature on sulfated zirconium oxide-catalyzed transesterification of triacetin with methyl alcohol (a) and curves of $\ln(\text{instantaneous triacetin concentration})/(\text{initial triacetin concentration})$ as a function of reaction time (b).^a Reaction conditions: triacetin:methyl alcohol molar proportion (1:20); catalyst load (5 wt%)

constants (k) for each process at each temperature were measured (Table 1). The resulting linear equations presented higher linear correlation coefficients (R^2) for the first-order equation, thus indicating that the reaction has first-order dependence in relation to the triacetin concentration at any temperature.

The angular coefficient (E_a/R) obtained by plotting $\ln k \times 1/T$ (K) (Eq. 2; Fig. 5) provided the activation energy (E_a) of the sulfated zirconium oxide-catalyzed transesterification of triacetin with methyl alcohol.

$$\ln k = \ln A - \left(\frac{E_a}{R}\right) \left(\frac{1}{T}\right) \quad (2)$$

The value of the activation energy dictates whether the reaction rate depends on the mass transfer phenomenon or chemical dependence. It was reported that the activation energy for the reactions that are limited by the mass transfer/diffusion processes is of the order of 10^{-15} kJ mol $^{-1}$ (Shi et al., 2016). Herein, the activation energy of the sulfated zirconium oxide-catalyzed transesterification reaction of the triacetin with methyl alcohol was 58.2 kJ mol $^{-1}$, which indicates that the reaction rate was controlled by the chemical processes (Fig. 5).

Effect of Catalyst Load on the SZr-Catalyzed Transesterification of Triacetin with Methyl Alcohol

To assure that only the catalyst concentration was affecting the reaction rate, all the measurements were done very far from the equilibrium (i.e., within first hour of the reaction). The kinetic curves are shown in Fig. 6.

The kinetic curves displayed in Fig. 6 show that the reaction conversion carried out with catalyst load of 4 or 5 wt% was almost complete. The reaction conversions were enhanced with the increase of catalyst load; it is clear

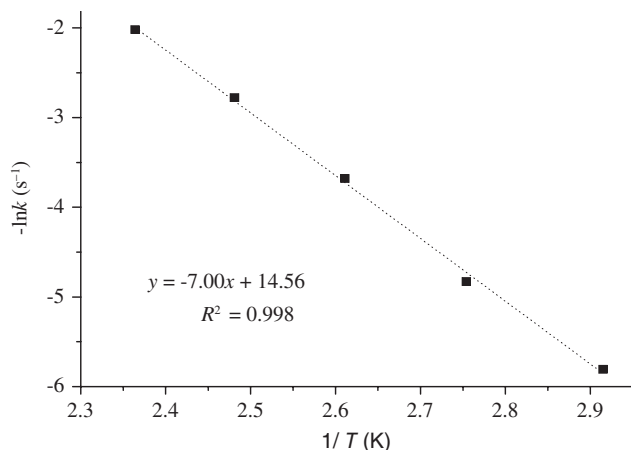


Fig. 5 Arrhenius plot of the sulfated zirconium oxide-catalyzed transesterification of triacetin with methyl alcohol

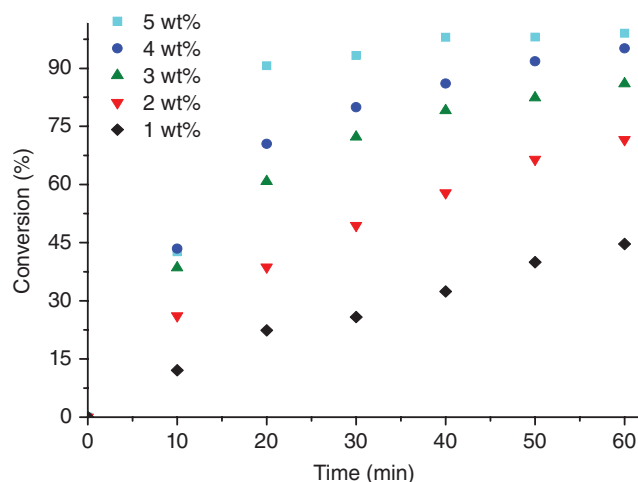


Fig. 6 Effect of catalyst load on sulfated zirconium oxide-catalyzed transesterification of triacetin with methyl alcohol^a. ^aReaction conditions: triacetin:methyl alcohol molar proportion (1:20); temperature (393 K)

evidence that the reactions did not reach the equilibrium. This effect can be attributed to the increase in the number of active sites due to high catalyst load.

Effects of Reactant Stoichiometry on the SZr-Catalyzed Transesterification of Triacetin with CH₃OH

The influence of the methanol:triacetin molar ratio in the reaction conversion is shown in Fig. SP5. The conversion of the triacetin improves with an increasing of the molar ratio and reaches a maximum (ca. 99%) when the proportion is 20:1 between alcohol and triacetin.

Despite the positive effect provoked by an increase of methyl alcohol excess of 9:1 to 12:1, the differences in conversions are minimal when comparing the proportions of 3:1 to 9:1. The results also show that the 12:1 stoichiometry becomes economically more interesting in terms of application potential (i.e., initial investment and operating cost), considering that the results are close to the highest molar ratio studied in this work.

Studies of Recovery and Reuse of the Sulfated Zirconium Oxide Catalysts

The main advantage of the heterogeneous catalysts over homogeneous ones is their ease of recovery and the possibility of reuse. In this work, deactivation studies were carried out aiming to evaluate the reusability of sulfated zirconium oxide. Fig. 7 shows the results of four successive recycles.

The catalyst activity showed a significant decrease after it was recovered and reused twice. The reactions with the first and second recycle achieved conversions of 99%. In

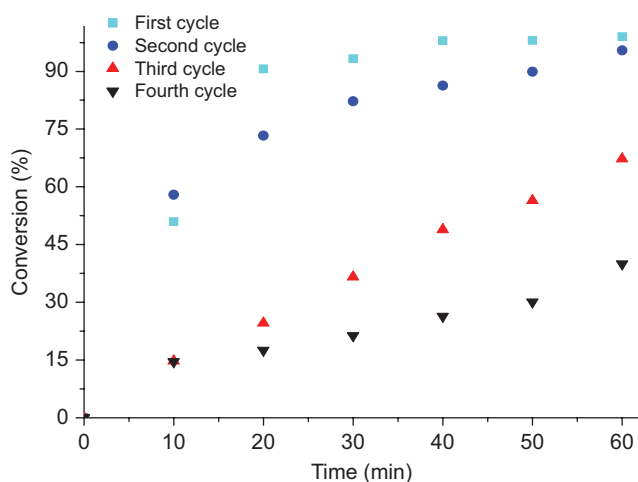


Fig. 7 Conversion of triacetin after recovery and reuse of sulfated zirconium oxide. ^aReaction conditions: triacetin:methyl alcohol molar proportion (1:20); temperature (393 K), catalyst (5 wt%)

the third and fourth recycles there was a significant decrease (ca. 67% and 39%, respectively).

The SZr catalysts were characterized after the reuse in each reaction cycle to study the possible changes in their properties. However, the diffractograms of the original sample and the reused catalysts were similar, indicating that the crystalline phase remained without significant modifications (Fig. 8).

The FT-IR spectra of the reused catalysts were like the original one. Only a little change was observed; the peak at 1080 cm^{-1} wavenumber underwent a split in two other peaks (Fig. SP6). Interestingly, this modification was also observed when the fresh catalysts was subjected to the procedure of washing and drying, even though it was not used.

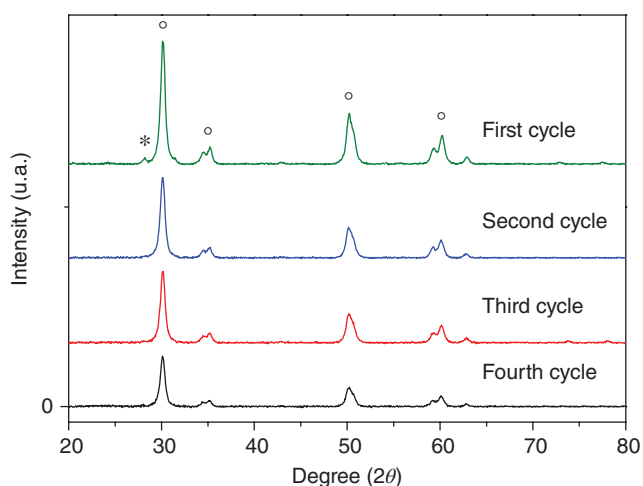


Fig. 8 Powder X-ray diffraction patterns of sulfated zirconium oxide fresh and after three reuse (°) the tetragonal phase and (*) the monoclinic phase

Table 2 Elemental analysis (SEM/EDS) of the sulfated zirconium oxide catalyst samples

Atom	Fresh	After first cycle	After second cycle	After third cycle
O	72.39	70.22	70.03	68.30
S	11.18	9.24	8.80	6.74
Zr	16.43	20.14	21.17	24.95

It means that there is no loss or noticeable alteration of the sulfate ions and that no organic species were adsorbed on the surface of the reused catalysts.

Our results agree with those described by Garcia et al. (2008), which demonstrated that the limitation of SZr is its quick deactivation. Those authors assessed the transesterification of vegetal oils over sulfated zirconium oxide and verified that the fatty-acid methyl esters yields dropped off strongly when they recycled the catalyst. The yields were decreasing as follows: 99%, 59%, 30%, and 14%. Although our catalyst has also been deactivated, it was more stable (ca. 99%, 97%, 69%, and 33% in the fourth cycle).

According to Corma, this deactivation is a drawback inherent to sulfated metal oxides and is a consequence of hydrolysis of sulfate groups, which are lost due to the water generated in the reactions (Corma, 1997). However, Kiss, Dimian, and Rothenberg (2006) reported that only a small loss of sulfate groups was detected when the water was at low concentration.

Therefore, to verify if the structural properties of SZ catalysts were affected during the recycle steps, we performed elemental analyses using EDS and their recorded SEM images before and after the reuse (Table 2 and Fig. SP7).

The comparison of SEM images of the fresh catalyst after the first use shows that no significant change occurred (Fig. SP7a,b). It is corroborated by elemental analysis of these catalysts, which were similar (Table 2). Nonetheless, the SEM images of the catalyst after second reuse (Fig. SP7c) show that both the crystallite size and rugosity were very distinct from the fresh catalyst.

Interestingly, the sulfur percentage of the samples after first and second reuse was close (ca. 9.24% and 8.80%; Table 2). However, the conversions achieved in the reactions with these catalysts were 97% and 69%, respectively (Fig. 7). It means that both structural properties and sulfur content play an important role in the catalytic activity.

Based on these results, we concluded that an acid-washing step is required to reactivate the acid strength of the catalyst. Thus, we performed an additional procedure after the removal of the catalyst from the reaction solution; the catalyst was washed three times with a mixture of methanolic sulfuric acid solution and then dried in an oven as in the initial procedure. The reaction performed reusing the acid-

treated catalyst resulted in no significant loss of activity with conversion reaching 95%. This was an efficient procedure that kept constant the catalytic activity of SZr.

Conclusion

The method used in the synthesis of the catalyst was efficient considering the results of FT-IR, XRD, and SEM/EDS. The experiments to evaluate the activity of the sulfated zirconium oxide catalyst in the transesterification reaction of triacetin with methyl alcohol reached high conversions (ca. 99%) under optimized conditions; 393 K, catalyst load ca. 5 wt%, and the molar ratio of triacetin to alcohol equal to 1:20. A first-order dependence in relation to the triglyceride concentration was obtained in the kinetic studies performed aiming to determine the rate constant by adjusting the experimental data. It was observed that the rate constant increased proportionally with an increase in temperature and the activation energy was 58.2 kJ mol⁻¹. The characterization of the reused catalyst did not reveal a significant change in its properties, however, after it was recycled twice there was a significant reduction in the catalytic activity. This drawback was overcome by performing an acid washing of the catalyst, which reactivated the acid sites of the catalyst.

Acknowledgments Authors thank the CAPES, FAPEMIG e CNPq.

Conflict of Interest The authors declare that they have no conflicts of interest.

References

- Bandyopadhyay, M., Tsunoji, N., & Sano, T. (2017) Mesoporous MCM-48 immobilized with aminopropyltriethoxysilane: A potential catalyst for transesterification of triacetin. *Catalysis Letters*, **147**:1040–1050.
- Basahel, S. N., Ali, T. T., Mokhtar, M., & Narasimharao, K. (2010) Influence of crystal structure of nanosized ZrO₂ on photocatalytic degradation of methyl orange. *Nanoscale Research Letters*, **10**:73–85.
- Brum, S. S., Santos, V. C., Destro, P., & Guerreiro, M. C. (2011) Esterificação de ácidos graxos utilizando zircônia sulfatada e compostos carvão ativado/zircônia sulfatada como catalisadores. *Quim Nova*, **34**:1511–1516.
- Chantrasa, A., Phlernjai, N., & Goodwin, J. G. (2011) Kinetics of hydrothermal-catalyzed transesterification of tricaprilyn and methanol for biodiesel synthesis. *Chemical Engineering Journal*, **168**:333–340.
- Corma, A. (1997) Solid acid catalysts. *Current Opinion in Solid State & Materials Science*, **2**:63–71.
- Delesma, C., Castillo, R., Sevilla-Camacho, P. Y., Sebastian, P. J., & Muñiz, J. (2017) Density functional study on the transesterification of triacetin assisted by cooperative weak interactions via a gold heterogeneous catalyst: Insights into biodiesel production mechanisms. *Fuel*, **202**:98–108.
- Dosuna-Rodríguez, I., Adriany, C., & Gaigneaux, E. M. (2011) Glycerol acetylation on sulphated zirconia in mild conditions. *Catalysis Today*, **167**:56–53.
- Furuta, S., Matsuhashi, H., & Arata, K. (2006) Biodiesel fuel production with solid amorphous-zirconia catalysis in fixed bed reactor. *Biomass and Bioenergy*, **30**:870–873.
- Garcia, C., Teixeira, S., Marciniuk, L., & Schuchardt, U. (2008) Transesterification of soybean oil catalyzed by sulfated zirconia. *Bioresource Technology*, **99**:6608–6613.
- Grossi, C. V., Jardim, E. O., de Araújo, M. H., Lago, R. M., & da Silva, M. J. (2010) Sulfonated polystyrene: A catalyst with acid and superabsorbent properties for the esterification of fatty acids. *Fuel*, **89**:257–259.
- Heshmatpour, F., & Aghakhanpour, R. B. (2011) Synthesis and characterization of nanocrystalline zirconia powder by simple sol-gel method with glucose and fructose as organic additives. *Powder Technology*, **205**:193–200.
- Hwang, K. S., Jeon, Y. S., Kim, S. B., Kim, C. K., Oh, J. S., An, J. H., & Kim, B. H. (2003) Ca-doped ZrO₂ thin films deposited by using the spin-coating pyrolysis process with a metal naphthenate precursor. *Journal of the Korean Physical Society*, **43**:754–757.
- Ibrahim, M. M. (2015) Photocatalytic activity of nanostructured ZnO–ZrO₂ binary oxide using fluorometric method. *Spectrochimica Acta A: Molecular and Biomolecular Spectroscopy*, **145**:487–492.
- Imi, M., Hommes, A., Winkelman, J. G. M., Hidayat, C., & Heeres, H. J. (2016) Kinetic studies on the transesterification of sunflower oil with 1-butanol catalyzed by *Rhizomucor miehei* lipase in a biphasic aqueous-organic system. *Biochemical Engineering Journal*, **114**:110–118.
- Intarapong, P., Luengnaruemitchai, A., & Jai-In, S. (2012) Transesterification of palm oil over KOH/NaY zeolite in a packed-bed reactor. *International Journal of Renewable Energy Research*, **1**:271–280.
- Ivanova, T., Harizanova, A., Koutzarova, T., & Vertruyen, B. (2010) Effect of annealing temperatures on properties of sol-gel grown ZnO–ZrO₂ films. *Crystal Research and Technology*, **45**:1154–1160.
- Jacobson, K., Gopinath, R., Meher, L. C., & Dalai, A. K. (2008) Solid acid catalyzed biodiesel production from waste cooking oil. *Applied Catalysis B: Environmental*, **85**:86–91.
- Jayakumar, S., Ananthapadmanabhan, P. V., Perumal, K., Thiyagarajan, T. K., Mishra, S. C., Su, L. T., ... Guo, J. (2011) Characterization of nano-crystalline ZrO₂ synthesized via reactive plasma processing. *Materials Science and Engineering B*, **176**:894–899.
- Jitputti, J., Kitiyanan, B., Rangsunvigit, P., Bunyakiat, K., Attanatho, L., & Jenvanitpanjakul, P. (2006) Transesterification of crude palm kernel oil and crude coconut oil by different solid catalysts. *Journal of Chemical Engineering*, **116**:61–66.
- Kamaruzaman, M. R., & Chin, S. Y. (2014) Synthesis and characterization of zirconium phosphate as a solid catalyst for esterification of wastewater containing acrylic acid. *Journal of Applied Sciences*, **14**:1339–1342.
- Kiss, A. A., Dimian, A. C., & Rothenberg, G. (2006) Solid acid catalysts for biodiesel production – Towards sustainable energy. *Advanced Synthesis and Catalysis*, **348**:75–85.
- Lughi, V., & Sergio, V. (2010) Low temperature degradation-aging-of zirconia: A critical review of the relevant aspects in dentistry. *Dental Materials*, **26**:807–820.
- Mardhiah, H. H., Ong, H. C., Masjuki, H. H., Lim, S., & Pang, Y. L. (2017) Investigation of carbon-based solid acid catalyst from *Jatropha curcas* biomass in biodiesel production. *Energy Conversion and Management*, **144**:10–17.
- Miao, Z., Zhou, J., Zhao, J., Liu, D., Bi, X., Chou, L., & Zhuo, S. (2017) A novel mesoporous sulfated zirconium solid acid catalyst

- for Friedel-Crafts benzylolation reaction. *Applied Surface Science*, **411**:419–430.
- Muñiz, J., Castillo, R., Robles, J. B., & Sansores, E. (2016) Density functional theory study of the reactivity and electronic structure of the transesterification of triacetin in biodiesel production via a sulfated zirconia heterogeneous catalysis. *International Journal of Quantum Chemistry*, **116**:988–999.
- Nakatake, D., Yazaki, R., Matsushima, Y., & Ohshima, T. (2016) Transesterification reactions catalyzed by a recyclable heterogeneous zinc/imidazole catalyst. *Advanced Synthesis and Catalysis*, **358**:2569–2574.
- Noda, L. K., Gonçalves, N. S., de Borba, S. M., & Silveira, J. A. (2007) Raman spectroscopy and thermal analysis of sulfated ZrO₂ prepared by two synthesis routes. *Vibrational Spectroscopy*, **44**:101–107.
- Park, Y. M., Chung, S., Eom, H. J., Lee, J., & Lee, K. (2010) Tungsten oxide zirconia as solid superacid catalyst for esterification of waste acid oil (dark oil). *Bioresource Technology*, **101**:6589–6593.
- Park, Y. M., Lee, D. W., Kim, D. K., Lee, J., & Lee, K. Y. (2008) The heterogeneous catalyst system for the continuous conversion of free fatty acids in used vegetable oils for the production of biodiesel. *Catalysis Today*, **131**:238–243.
- Pereira, K. R. O., Júnior, A. U. A., Carvalho, M. W. N. C., & Silva, A. S. A. (2015) Síntese e caracterização de materiais do tipo MCM-41 sulfatada. *Blucher Chem Proceedings*, **3**:1069–1079.
- Pizzio, L. R., Vásquez, P. G., Cáceres, C. V., & Blanco, M. N. (2003) Supported Keggin type heteropolycompounds for ecofriendly reactions. *Applied Catalysis A*, **256**:125–139.
- Pradhan, P., Chakraborty, S., & Chakraborty, R. (2016) Optimization of infrared radiated fast and energy-efficient biodiesel production from waste mustard oil catalyzed by Amberlyst 15: Engine performance and emission quality assessments. *Fuel*, **173**:60–68.
- Ranjbar, M., Yousefi, M., Lahoooti, M., & Malekzadeh, A. (2012) Preparation and characterization of tetragonal zirconium oxide nanocrystals from isophthalic acid-zirconium (IV) nanocomposite as a new precursor. *International Journal of Nanoscience and Nanotechnology*, **8**:191–196.
- Rouquerol, F., Rouquerol, J., & Sing, K. (1999) *Adsorption by powders and porous solids: Principles, methodology and application*. London: Academic Press.
- Saravanan, K., Tyagi, B., & Bajaj, H. (2014) Catalytic activity of sulphated zirconia solid acid catalyst for esterification of myristic acid with methanol. *Indian Journal of Chemistry*, **53A**:799–805.
- Shi, G., Yu, F., Wang, Y., Pan, D., Wang, H., & Li, R. (2016) A novel one-pot synthesis of tetragonal sulfated zirconia catalyst with high activity for biodiesel production from the transesterification of soybean oil. *Renewable Energy*, **92**:22–29.
- Sigwadi, R. A., Mavundla, S. E., Moloto, N., & Mokrani, T. (2016) Synthesis of zirconia-based solid acid nanoparticles for fuel cell application. *Journal of Energy in Southern Africa*, **27**:60–67.
- Silva, F. N., Moura, T. F. B., Silva, A. S., Pallone, E. M. J. A., & Costa, A. C. F. M. (2017) Preparation and characterization of sulfated zirconia acid catalysts for application in the esterification of cottonseed oil. *Ceramic*, **63**:402–412.
- Silva, V. W. G., Laier, L. O., & da Silva, M. J. (2010) Novel H₃PW₁₂O₄₀: Catalysed esterification reactions of fatty acids at room temperature for biodiesel production. *Catalysis Letters*, **135**:207–211.
- Son, J. R., Gwon, T. D., & Kim, S. B. (2001) Characterization of zirconium sulfate supported on zirconia and activity for acid catalysis. *Bulletin of the Korean Chemical Society*, **22**:1309–1315.
- Sun, Y., Ma, S., Du, Y., Yuan, L., Wang, S., Yang, J., ... Xiao, F. S. (2005) Solvent-free preparation of nanosized sulfated zirconia with Brønsted acidic sites from a simple calcination. *The Journal of Physical Chemistry B*, **109**:2567–2572.
- Wang, Y. Y., & Chen, B. H. (2016) High-silica zeolite beta as a heterogeneous catalyst in transesterification of triolein for biodiesel production. *Catalysis Today*, **278**:335–343.
- Yu, S., Jiang, P., Dong, Y., Zhang, P., Zhang, Y., & Zhang, W. (2012) Hydrothermal synthesis of nanosized sulfated zirconia as an efficient and reusable catalyst for esterification of acetic acid with n-butanol. *Bulletin of the Korean Chemical Society*, **33**:524–528.
- Zabeti, M., Daud, W. M. A. W., & Aroua, M. K. (2009) Activity of solid catalysts for biodiesel production: A review. *Fuel Processing Technology*, **90**:770–777.
- Zieba, A., Drelinkiewicz, A., Chmielarz, P., Matachowski, L., & Stejskal, J. (2010) Transesterification of triacetin with methanol on various solid acid catalysts: A role of catalyst properties. *Applied Catalysis A*, **387**:13–25.